Evaluating Future Climate Projections in Upper Indus Basin through GFDL-ESM2M Model

Faiza Sarwar[1], Fareeha Tariq[2], Muhammad Shareef Shazil[2], Saira Batool[3], Nadia Mehrdin[4], Samreen Javed[2], Syed Amer Mahmood[2]*

[1] Institute of Geography, University of the Punjab, Lahore, Pakistan
[2] Department of Space Science, University of the Punjab, Lahore, Pakistan
[3] Centre for Integrated Mountain Research (CIMR), University of the Punjab, Lahore, Pakistan
[4] Deapartment of Kashmir Studies, University of the Punjab, Lahore, Pakistan
*Correspondence: shazil.spacescience@gmail.com

Citation | Sarwar.F, Tariq.F, Shazil.M.S, Batool.S, MehrdinN, Javed.S, Mahmood.S.A "Evaluating Future Climate Projections in Upper Indus Basin through GFDL-ESM2M Model, IJIST, Vol. 5 Issue. 4 pp 440-460, Oct 2023

Received | Sep 04, 2023; **Revised** | Oct 20, 2023; **Accepted** | Oct 24, 2023; **Published** | Oct 25, 2023.

This study aims to examine the future climate projections in the Upper Indus Basin (UIB). The Global Climate Model (GFDL-ESM2M) data was utilized to analyze two variables, namely precipitation and temperatures. The study focused on three distinct time periods: near century (2020-2040), mid-century (2041-2070), and end of century (2071-2099). This process involved the utilization of a downscaling technique that relied on the RCP4.5 scenario. The Mann-Kendall (MK) and Sen's slope estimate test will be employed to analyze the parameters of temperature and precipitation, enabling the identification of yearly, seasonal, and monthly patterns. The application of the MK and Sen's slope estimate approaches revealed a lack of statistical significance in the observed upward trend in yearly precipitation and temperature. Over the course of nearly a century, the average Coefficient of Variation for temperature exhibited a range of -67.5% to 308.9%. During the midcentury period, there was observed variation in the mean monthly rainfall across all months. Notably, the month of March exhibited the highest average rainfall of 274.2mm, while September had the lowest average rainfall of 31.9mm. The data exhibited a positive skewness, suggesting that there was a tendency for higher levels of rainfall towards the end of each month compared to the beginning. The data indicates that there is an upward trend in precipitation throughout the midcentury period in comparison to the near century, but a downward trend is observed towards the conclusion of the century. The temperature readings exhibit a constant upward trend from the early part of the century to the middle of the century, followed by a subsequent increase from the middle of the century to the end of the century. Furthermore, the data revealed that the highest amount of precipitation is experienced during the spring season, whereas the lowest amount of rainfall is recorded during autumn throughout all temporal intervals.

Abbreviations

Intergovernmental Panel on Climate Change (IPCC)
Hindu Kush Himalayas (HKH)
Upper Indus Basin (UIB)
Hindu Kush Himalayas (HKH)
Representative Concentration Pathways (RCPs)
Regional Climate Model (RCM)
Million Acre-Feet (MAF)
Mann-Kendall (MK)
Jhelum River Basin (JRB)
World Meteorological Organization (WMO)
Near Century Research (NCR)
Coefficient of Variation (CV %)
Standard Deviation (SD)

Keywords: Global Climate Model, GFDL-ESM2M, Representative Concentration Pathways (RCPs), Future Projections.

Introduction:

The role of climate in human existence is of paramount importance, as it exhibits a profound interconnection with both beneficial and detrimental consequences on various facets of society and the economy [1]. The climate holds significant relevance as it exerts a deep influence on all facets of existence on our planet. Their primary objective is to generate the necessary knowledge to foster the development of sustainable livelihoods for individuals [2]. Climate change represents an intrinsic component of weather systems, manifesting as a natural phenomenon. In recent years, there has been a significant surge in attention towards climate change due to its profound implications for ecosystems and water resources [3]. The primary factor contributing to this phenomenon is human activity, specifically the emission of gases into the atmosphere, resulting in the greenhouse effect, heat retention, and ultimately global warming. Climate change poses significant threats and challenges to global ecosystems, civilizations, and economies [4].

The progressive increase in global temperatures is a consequence of the rising quantities of greenhouse gases, which lead to the enhanced trapping of heat within the Earth's atmosphere [5]. The increase in temperature associated with global warming has extensive ramifications for the climate system, resulting in a multitude of repercussions. The data presented by the Intergovernmental Panel on Climate Change (IPCC) emphasizes the pressing necessity for global initiatives aimed at reducing greenhouse gas emissions, addressing the consequences of climate change, and striving towards a sustainable future [6]. Moreover, alterations in land utilization, such as the conversion of forested areas into agricultural land, have the potential to liberate sequestered carbon and so contribute to the phenomenon of climate change [7].

The occurrence of extreme events is not evenly distributed across the Earth, as certain places exhibit more susceptibility to the fluctuations of climatic extremes compared to others. Over the past five years, Pakistan has experienced significant impacts from severe floods and heat waves [8]. The water cycle is influenced by climate, encompassing factors such as precipitation patterns, snowmelt, and the availability of water. The fluctuations in temperature and precipitation patterns in mountainous areas exert a significant influence on the availability of water resources for downstream drainage basins. [3]. The variability of climatic feedback is contingent upon the spatial distribution of surface temperature alterations, resulting in non-constant radiative feedback and sensitivity [9]. Temperature trends are undergoing alterations as a consequence of global warming, predominantly driven by the escalating concentrations of greenhouse gases in the Earth's atmosphere [10]. There is a consensus among scientists that the average global surface temperature has increased by approximately 0.25 to 0.60 °C in the past century. This phenomenon is widely attributed to the intensified greenhouse effect, which is believed to be a consequence of the escalating levels of carbon dioxide and other greenhouse gases in the Earth's atmosphere. The observed upward trajectory, nonetheless, exhibits notable temporal and regional fluctuations [11]. Global mean temperatures have displayed a continuous upward trajectory and are anticipated to endure, giving rise to a multitude of consequences. The frequency and intensity of heat waves and extreme heat events are escalating progressively, posing significant risks to human health, agriculture, and ecosystems [12]. The winter season is experiencing a trend towards less severe cold temperatures, resulting in a decrease in the occurrence of extreme cold events. This phenomenon has notable implications for snowfall patterns and various activities associated with the winter season. The polar regions experience amplified temperature rises, which accelerate the melting of glaciers and contribute to the elevation of global sea levels [13].

The Indus, Jhelum, and Chenab rivers originate from the Hindu Kush Himalayas (HKH) and play a crucial role in facilitating agricultural activities, hence serving as a vital resource for Pakistan's agricultural industry [15]. The effective management and optimal usage of water

resources derived from the UIB play a crucial role in enhancing agricultural output and fostering economic development within the nation.

Various General Circulation Models (GCMs) have been employed to generate future climate projections based on multiple Representative Concentration Pathways (RCPs), specifically RCP 4.5 and 8.5. However, it is important to note that there are significant variations in the choice of underlying GCM or Regional Climate Model (RCM), as well as the techniques employed for bias-correction and downscaling of these projections [16]. Every study conducted in the UIB represents a distinct manifestation of the expected hydro-climatology. This is influenced by various factors including the data sources utilized, the methodology employed, and the specific modeling techniques employed. It is important to note that considerable uncertainties are introduced at each stage of data processing and simulation within each study. The consensus among numerous studies is that future temperature is expected to rise, precipitation will become more intense, stream flow will increase, and there will be a greater frequency and intensity of extreme weather events. The alterations being made will result in hydrological consequences within the UIB [17].

Study Area:

Upper Indus Basin:

UIB is derived from the geological formations of the Hindu HKH mountain ranges. The UIB is a vast geographical expanse characterized by its lack of precise demarcation through particular latitude and longitude measurements. However, it is often situated within the latitudinal range of 31° to 37° North and the longitudinal range of 73° to 79° East. The above coordinates offer a first approximation of the geographical extent of the UIB region. The geographical area under question encompasses elevated portions in northern Pakistan, northern India, and certain parts of China. The basin spans across the regions of Gilgit-Baltistan in Pakistan, Ladakh in India, and the Tibetan Plateau in China. The geographical location of this area is situated in the northwestern portion of the Indian subcontinent. It is demarcated by the Karakoram Range in the northwest, the Himalayas in the southwest, and the Tibetan Plateau in the east.

Jhelum River Basin:

The Jhelum River and its tributaries are encompassed within the Jhelum River Basin (JRB), situated in the Himalayan-mountain range. The monsoon circulation system in the region is influenced by the Arabian Sea, Indian Ocean, and Bay of Bengal [18]. The Jhelum River primarily traverses the Indian subcontinent, moving across the territories of both India and Pakistan. This river holds significant importance within the Indus River system. The Jhelum River originates from the Verinag region located within the Indian Union territory of Jammu and Kashmir. Subsequently, the river traverses the Kashmir Valley, through urban and rural areas within the jurisdiction of Indian-administered Jammu and Kashmir, including Srinagar, Baramulla, and Uri. The aforementioned route traverses the Line of Control and proceeds into Azad Kashmir, which is under Pakistani administration. It thereafter passes through the districts of Mirpur and Jhelum. Ultimately, it converges with the Chenab River in the Punjab area of Pakistan, namely near Trimmu.

In general, the Jhelum River traverses a considerable expanse through the territories of India and Pakistan, exerting a significant influence on the local people situated along its course. The Jhelum River and its associated watershed region undergo increased river flows due to the substantial precipitation brought by the southwest monsoon throughout the summer season. The Mangla Dam, which is the second largest dam in Pakistan and a significant contributor to the country's hydroelectric generation, serves as a reservoir for water originating from the Jhelum, Chenab, and Indus Rivers. The Mangla dam, has a storage capacity of roughly 7.4 Million Acre-Feet (MAF), serves as a crucial source of agricultural water within the Indus Basin.

Impacts:

The hydrological patterns of rivers are influenced by variations in temperature and precipitation within the atmosphere, particularly in basins characterized by significant snow accumulation [3][19]. The influence of temperature fluctuations on seasonal water supplies has been demonstrated, while alterations in runoff volumes and snow accumulation have been observed to affect precipitation in the SRIR [20][21]. The annual precipitation in the SRIR is seeing a notable upward trend, with an increase of approximately 36.6 mm per decade specifically observed in the JRB. Furthermore, it has been indicated that there is an increase in temperature in the UIB. The hydrological regimes of the UIB are affected by a range of implications resulting from the long-term alterations in temperature and precipitation [22].

It is crucial to comprehend the magnitudes and regional disparities of these alterations, given that the sustenance of numerous individuals is dependent upon these water resources. Through the analysis of deviations from typical hydro-climatological factors, we may improve our ability to plan and prepare for the inevitable repercussions of these alterations. The adoption of a proactive strategy will facilitate the development of efficient methods for water resource management, with the aim of mitigating potential socio-economic and environmental consequences [23]. Figure 1 shows the map for area of interest.

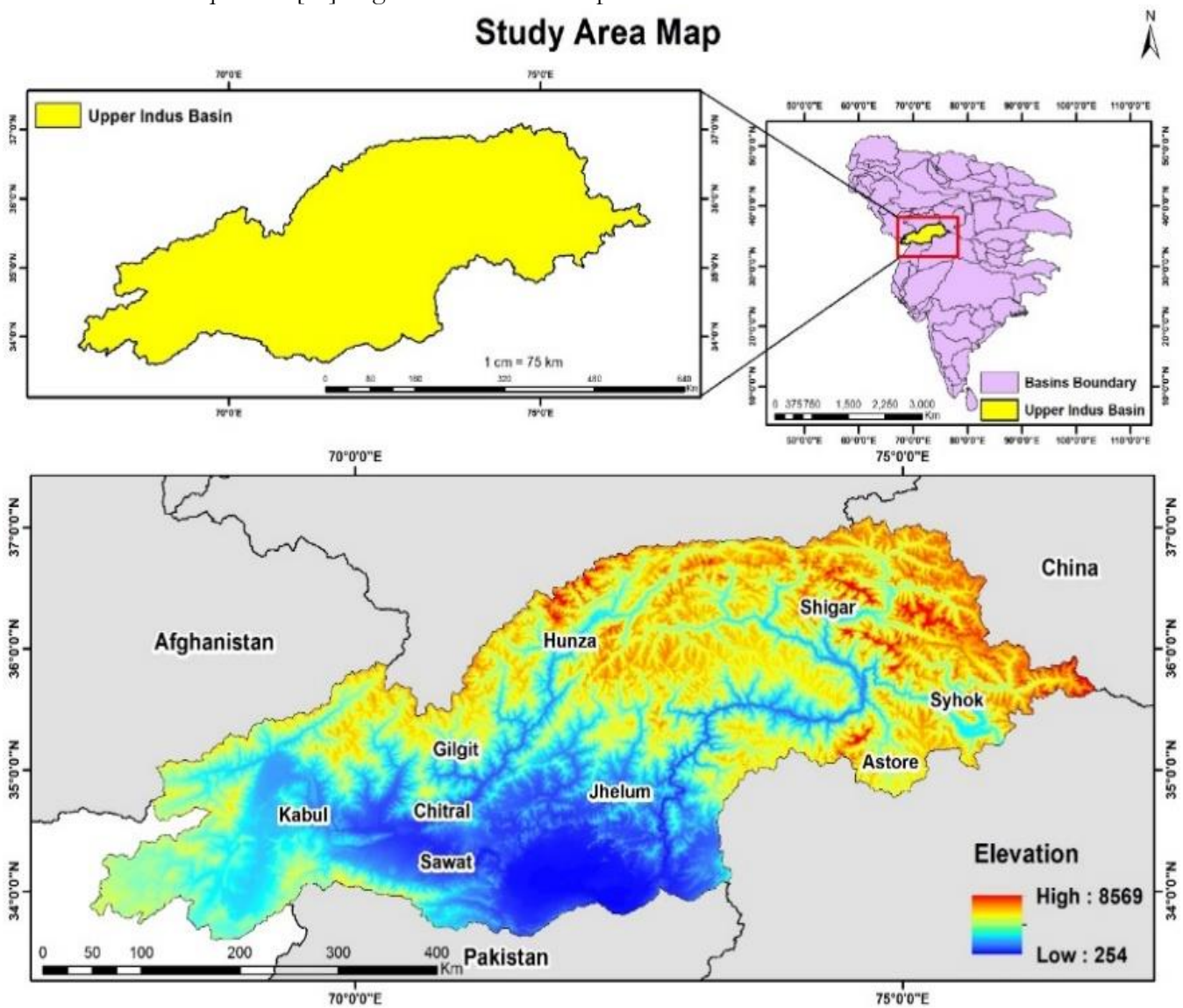

Figure 1 Study Area Map

One other noteworthy feature of this study is the application of climate change projections to model the prospective hydrology of the UIB. Various GCMs have generated future climate forecasts based on multiple " RCPs," specifically RCP 4.5 and 8.5. However, there are notable differences in the fundamental GCM or RCM utilized to generate these projections, as well as the methodologies employed for bias correction and downscaling [16]. Each study represents a distinct representation of the expected hydro-climatology in the UIB, influenced by the data sources, methodology, and modeling methodologies employed. Significant uncertainties are acknowledged at each stage of data processing and simulation in all of the studies. The majority of research findings align with prevailing trends, indicating an expectation of elevated future temperatures, increased precipitation, heightened stream flow, and a larger frequency of severe weather events associated with these climatic factors. The aforementioned modifications will result in hydrological consequences within the UIB [17].

Material and Methods:

Data Collection:

The collection of data pertaining to the monthly average precipitation and temperature in the Jhelum Indus basin from 2020 to 2099 was conducted utilizing the GCM known as GFDL-ESM2M. The selection of precipitation and temperature as variables was based on their fundamental role in exerting a considerable influence on the climate system. The data that has been gathered offers significant insights into the expected alterations in temperature and precipitation patterns within the stated timeframe in the Jhelum Indus basin. The examination of this data has provided valuable insights into the probable ramifications of climate change on the hydrological and climatic conditions in the surrounding area.

Methodology:

The principal objective of this research endeavor was to assess forthcoming climate estimates pertaining to the UIB within the timeframe spanning from 2020 to 2099. The time range was categorized into three distinct groups in the study: the near future (2020-2040), the midcentury (2041-2070), and the end of the century (2071-2099). The primary objective of this study was to analyze the patterns of temperature and precipitation variations and their subsequent influence on stream flows. The investigation primarily concentrated on the Jhelum River, which holds significant importance as one of the prominent rivers within the designated research region.

Mann-Kendall Test:

The Mann-Kendall (MK) test is a non-parametric test used for the analysis of trends. The statistical test in question was initially proposed by Mann in 1945, and later Kendall computed the distribution of the test statistic in 1975. The Mann-Kendall test is commonly utilized to assess trends in time series data, particularly when the underlying data does not adhere to a certain distribution. The method is particularly advantageous in identifying monotonic trends, whether they exhibit an upward or downward trajectory, without making any assumptions regarding the distribution of the data. The determination of the significance of trends in different variables over time can be achieved by computing the MK statistic and afterward comparing it to the appropriate distribution. The test established by the World Meteorological Organization (WMO) is utilized to analyze time series trends in ecological data [21]. This approach is suitable for situations in which the data exhibits seasonal patterns and has repetitive qualities. The Mann-Kendall test possesses various advantages, which can be enumerated as follows:

The nonparametric technique does not necessitate any assumptions about the distribution of data, hence eliminating the need for speculative assumptions in terms of data distribution. Consequently, there is a lack of ambiguity. The data on climate for a single month

or season can be readily applied. The MK trend test utilizes the below equation to calculate the statistic:

$$\mathbf{S} = \sum_{i=1}^{n-1} \sum_{j=i+1}^{n} \operatorname{sgn}(x_j - x_i) \quad \textbf{(1)}$$

Where n is the total amount of data indications, $\mathbf{x_i}$ and $\mathbf{x_j}$ are the order of the data values, and sgn (.) is the sign operation, which can possibly be figured as follows:

$$gn(x_j - x_i) = \begin{Bmatrix} 1x_j - x_i > 0 \\ 0x_j - x_i = 0 \\ -1x_j - x_i < 0 \end{Bmatrix} \quad \textbf{(2)}$$

A positive S number indicates an increasing trend, whereas a negative number shows a decreasing trend.

$$\operatorname{var}(s) = \frac{n(n-1)(2n+5) - \sum_{i=1}^{m} t_i(t_i-1)(2t_i+5)}{18} \quad \textbf{(3)}$$

When "m" represents the quantity of interconnected groups, each possessing a distinct assemblage of information. A bonded group refers to a collection of information entities that has identical values. The calculation of the adapted test statistic (Z_mk) is performed.

$$Z_{mk} = \begin{bmatrix} \frac{s-1}{\sqrt{\operatorname{Var}(S)}}, & S > 0 \\ 0, & S = 0 \\ \frac{S+1}{\sqrt{\operatorname{Var}(S)}}, & S < 0 \end{bmatrix} \quad \textbf{(4)}$$

In a two-sided trends test, the null hypothesis should be accepted if it demonstrates significance at the predetermined level of probability (α). The positive value of (Z_mk) indicates an increasing pattern, whereas the negative value of (Z_mk) signifies a decreasing pattern. The Mann-Kendall test statistic, denoted as (Z_mk), follows a standard normal distribution with a mean of 0 and a variance of 1. The aforementioned figure is representative of the P-value associated with a specific trend.

Sen's Slope Estimation:

This study employs the Theil-Sen (TS) methodology as a nonparametric alternative method for estimating the amplitude of trends. In contrast to the MK test, which does not yield an estimation of trend magnitudes, the TS technique is frequently favored for the quantification of trend slopes. The time series (TS) technique, which assumes a linear trend in hydro-meteorological time-series data, has been commonly employed to assess the strength of the trend. The process involves calculating the slopes (β) for all possible combinations of data.

$$\boldsymbol{\beta = \text{median}\left((x_j - x_k)/(j-k)\right)} \quad \textbf{(5)}$$

The Theil-Sen (TS) approach is utilized to determine trends in time series data. A positive value of the TS statistic indicates an upward (increasing) trend, while a negative value shows a downward (decreasing) trend. The slope value, typically computed by linear regression analysis, denotes the measure of the rate of change between two variables throughout a certain time period.

Results and Discussions:

Precipitation Trend Near Century (2020-2040):

Throughout the Near Century Research (NCR), various statistical parameters were calculated on a monthly basis, including the Mean, Variance, Standard Deviation, Kurtosis, Skewness, Range, Total Rainfall, Minimum Rainfall, and Maximum Rainfall (as shown in Table 1). According to the collected data, the average monthly rainfall exhibited variations, ranging from a minimum of 30.4mm in September to a maximum of 252.4 mm in March. During this particular time period, spanning nearly a century, the highest recorded level of precipitation in the month of April was 1054.9mm, while the lowest recorded level was in September, at 1.0mm. The Coefficient of Variation (CV%) for monthly rainfall, which represents the relative fluctuation of the data in relation to the mean, ranges from 57.2% to 122.4% on average. The

coefficient of variance was found to be highest in the month of November and lowest in the month of July. The research also indicates that a positive Skew value was observed for each month of the year, indicating that the amount of rainfall at the end of each month surpasses the amount of rainfall at the beginning of each month.

Table 1 Monthly precipitation statistics in near century (2020-2040)

Months	N	Mean	Max	Min	Range	Std.D	Var	Skew	Kurt	CV%
Jan	21	113.1	433.7	5.4	428.3	121.3	14716.3	1.6	2.0	107.3
Feb	21	119.3	448.1	10.0	438.2	106.4	11324.9	1.6	3.3	89.2
Mar	21	253.1	708.4	37.2	671.2	214.7	46078.7	0.9	-0.5	84.8
Apr	21	207.8	1054.9	7.0	1047.9	224.7	50497.7	2.8	10.3	108.1
May	21	75.0	233.1	21.3	211.8	51.3	2633.9	1.7	3.5	68.4
Jun	21	61.1	232.2	2.4	229.7	52.9	2798.7	1.8	4.5	86.6
Jul	21	206.3	468.9	10.6	458.3	117.0	13687.6	0.2	-0.3	56.7
Aug	21	76.2	267.6	7.5	260.1	65.0	4230.1	1.5	2.7	85.4
Sep	21	30.4	64.1	1.0	63.1	19.6	382.6	0.1	-1.0	64.3
Oct	21	38.9	93.8	4.4	89.4	25.2	635.7	0.4	-0.6	64.8
Nov	21	58.8	310.4	1.7	308.7	74.4	5530.3	2.3	6.1	126.5
Dec	21	127.3	573.4	3.8	569.6	137.9	19004.2	1.9	4.4	108.3
Annual	21	113.9	191.8	59.6	132.2	34.1	1164.9	0.6	0.5	30.0

The coefficient of kurtosis exhibited its highest value of 10.3 during the month of April, while the degree of skewness reached its lowest value of 0.1 in September. The calculated annual standard deviation was found to be 34.1, while the monthly standard deviation varied between 19.6 and 224.7. Furthermore, it is evident that the annual precipitation pattern during the entire duration of the study diverges from the customary distribution.

The winter and spring seasons, encompassing the months of December, January, February, March, and April, exhibit the highest levels of monthly precipitation, characterized by substantial rainfall. In contrast, the fall seasons, spanning September, October, and November, experience minimal precipitation, often referred to as the harvesting season and a period of aridity. According to the data presented in Table 1, the maximum annual rainfall recorded during a span of 21 years is 191.8mm, while the smallest annual rainfall is 59.6mm.

Figure 2 illustrates the temporal variability of average annual precipitation data over a span of nearly one hundred years. During the specified time frame, it is projected that the highest recorded amount of rainfall will reach 191.8mm in the year 2035, while the lowest recorded amount is anticipated to be 59.6mm in 2026.The data indicates a statistically insignificant upward trend in precipitation levels within the region.

Temperature Trend Near Century (2020-2040):

Different statistical tests have been used to evaluate the trend in monthly data for the near century analysis (2020-2040). The results have been calculated in Table 3 through preliminary data analysis.

The greatest temperature recorded during this specific time frame is 16.5°C in the month of June, while the minimum temperature is -6.0°C in January. The average monthly temperature throughout the year varies between -3.1°C and 13.4°C, with the highest recorded in July and the lowest in January. The annual standard deviation was determined to be 0.62, but the monthly standard deviation varied between 1.10 and 2.10.

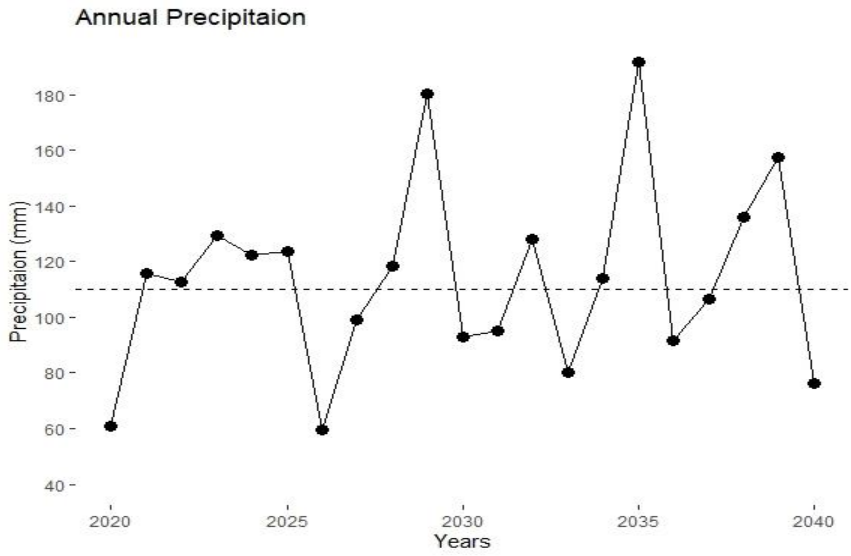

Figure 2 Annual precipitation trend for the period of near century (2020-2040)

Table 2 Monthly Mann-Kendall and Sen.'s slope results for precipitation in near century (2020-2040)

Months	Annual Precipitation			
	z-value	p-value	Kendall tau	Slope
Jan	0.63	0.53	0.10	1.81
Feb	0.09	0.93	0.02	0.31
Mar	-1.66	0.10	-0.27	-9.65
Apr	0.69	0.49	0.11	4.42
May	1.24	0.22	0.20	1.61
Jun	0.39	0.69	0.07	0.74
Jul	2.14	0.03	0.34	8.39
Aug	-0.63	0.53	-0.10	-1.42
Sep	1.18	0.24	0.19	1.04
Oct	2.20	0.03	0.35	2.20
Nov	-0.03	0.98	-0.01	-0.22
Dec	0.51	0.61	0.09	1.30
Annual	0.39	0.69	0.07	0.83

Table 3 Monthly Temperature statistics in near century (2020-2040)

Months	N	Mean	Max	Min	Range	Std.D	Var	Skew	Kurt	CV%
Jan	21	-3.1	-1.0	-6.0	5.0	1.3	1.8	-0.6	-0.2	-43.5
Feb	21	-2.5	0.4	-4.9	5.3	1.7	2.9	0.2	-1.3	-67.5
Mar	21	0.6	4.4	-3.3	7.7	2.0	3.8	-0.1	0.0	308.9
Apr	21	4.6	6.8	1.4	5.4	1.3	1.7	-1.1	1.7	28.4
May	21	9.3	12.6	4.8	7.8	2.1	4.2	-0.8	0.4	22.1
Jun	21	13.1	16.5	9.9	6.6	1.6	2.5	-0.2	0.3	12.0
Jul	21	13.4	15.8	11.4	4.5	1.3	1.7	0.2	-1.0	9.7
Aug	21	12.1	13.8	9.8	4.0	1.2	1.5	-0.8	-0.4	10.2
Sep	21	9.7	12.2	7.2	5.0	1.4	2.1	0.1	-1.2	14.9
Oct	21	4.9	6.9	2.4	4.4	1.4	2.0	-0.2	-1.3	28.8
Nov	21	1.7	7.1	-1.1	8.1	1.9	3.8	1.0	1.6	116.1
Dec	21	-2.2	-0.1	-4.4	4.3	1.1	1.1	0.1	-0.1	-48.9
Annual	21	5.1	6.3	3.8	2.5	0.6	0.4	-0.3	0.1	11.5

The region's yearly temperature shows uneven distribution, with positive and negative skewness. It's left-skewed, with the highest CV in March (-67.5% to 308.9%) and the lowest in February. Kurtosis ranged from -1.3 to 1.7: January, February, July, August, September, October, and December have negative kurtosis (flat distribution), while others have positive kurtosis (peaked distribution). See Table 3 for monthly and annual statistical values

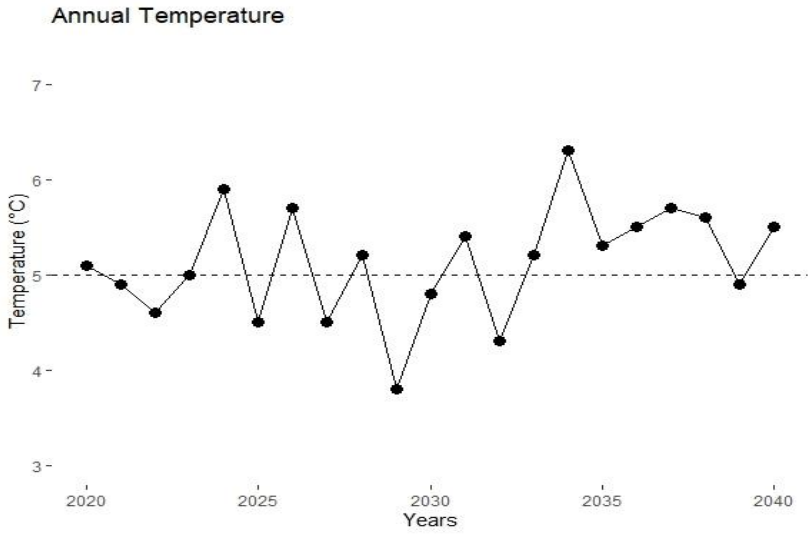

Figure 3 Annual Temperature trend for the period of near century (2020-2040)

Figure 3 illustrates the temporal variability of average yearly temperature data over a span of nearly one hundred years. The projected highest mean temperature for the given time is anticipated to reach 6.7°C in 2034, while the minimum is likely to be 3.8°C in 2029. The temperature in the area exhibits a statistically insignificant upward trend over the specified time period.

Figures 4 and 5 depict the trends in mean annual maximum temperature and lowest temperature, respectively. Figure 4 exhibits a modest upward trend during the specified time period. The mean maximum temperature exhibited fluctuations, ranging from 16.5°C in 2031 to 12.2°C in 2029. Figure 5 exhibits a pronounced upward trajectory that persists over the whole duration under consideration. The mean lowest temperature exhibited fluctuations ranging from -6.0°C in 2020 to -2.3°C in 2037.

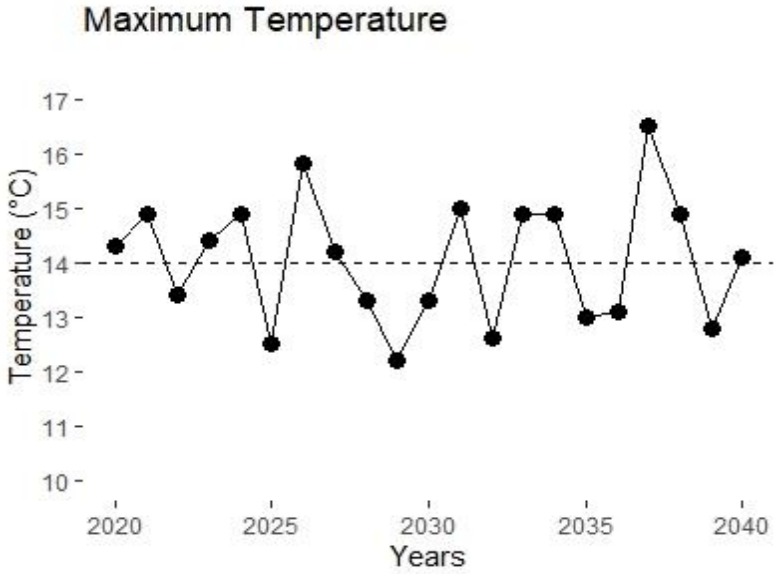

Figure 4 Annual Maximum Temperature trend for the period of near century (2020-2040)

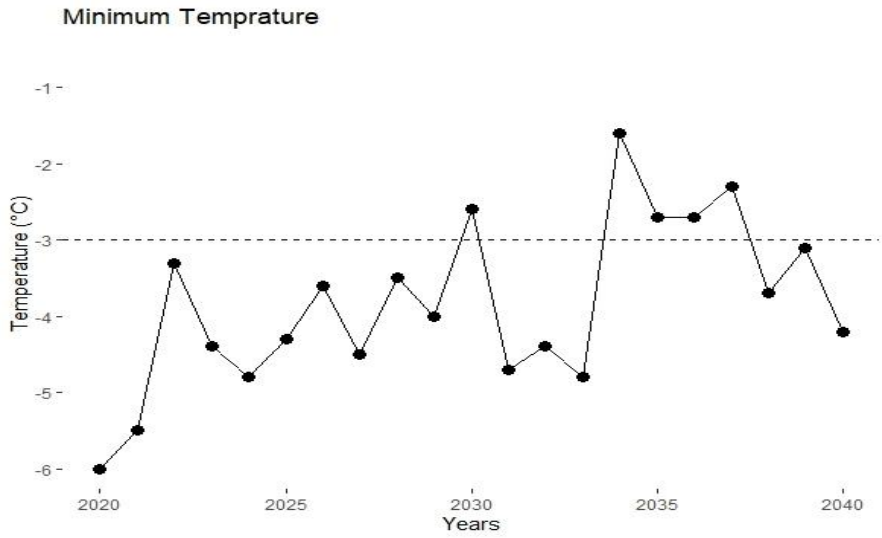

Figure 5 Annual Minimum Temperature trend for the period of near century (2020-2040)

The MK and Sen's slope estimate methodologies were utilized at a monthly resolution to examine the annual temperature data of the Jhelum Indus Basin, with the objective of detecting any prevailing trends. The determination of the trend was performed using the least significant level, which is the threshold at which the statistical significance of the trend is established at the stated confidence level. The data shown in Table 4 demonstrates a lack of statistical significance in the observed increase in annual temperature.

The p-values for the majority of the months indicate the presence of a discernible trend. Positive Kendall tau values were seen during the study period in the months of January-April, September- December. Negative Kendall tau values were seen in the months of May-August. During the designated period of analysis, a broadly inconsequential positive trend was found in the months of Jan-Apr, and Sep-Dec. Conversely, a generally inconsequential negative statistical trend was identified in the months of May-Aug, with a confidence level of 95% ($\alpha = 0.05$). The majority of the month exhibits a positive slope value, indicating an increasing tendency.

Table 4 Monthly MK and Sen.'s slope results of temperature in near century (2020-2040)

Months	Annual Temperature			
	z-value	p-value	Kendall tau	Slope
Jan	2.14	0.03	0.34	0.13
Feb	0.33	0.74	0.06	0.02
Mar	0.09	0.93	0.02	0.02
Apr	0.82	0.41	0.13	0.03
May	-0.15	0.88	-0.03	-0.01
Jun	-0.39	0.69	-0.07	-0.02
Jul	-0.75	0.45	-0.12	-0.04
Aug	-0.09	0.93	-0.02	0.00
Sep	0.00	1.00	0.00	0.00
Oct	1.36	0.17	0.22	0.07
Nov	0.09	0.93	0.02	0.01
Dec	2.63	0.01	0.42	0.11
Annual	1.36	0.17	0.22	0.03

Precipitation Trend Mid Century (2041-2070):

The Midcentury study analyzed monthly statistical parameters (Mean, Variance, SD, Kurtosis, Skewness, Range, Total rainfall, Min-Max rainfall) shown in Table 5. Precipitation varied monthly, from 31.9mm in September to 274.2mm in March. January had the highest

(895.5mm) and September had the lowest (0.1mm) rainfall. Monthly rainfall's CV% ranged from 63.6% to 114.5%, highest in January and lowest in October. Positive Skew values indicated more rainfall at month-end than at the beginning.

Table 5 Monthly precipitation statistics in midcentury (2041-2070)

Months	N	Mean	Max	Min	Range	Std.D	Var	Skew	Kurt	CV%
Jan	30	162.7	895.5	1.8	893.7	186.2	34682.7	2.5	7.7	114.5
Feb	30	143.0	753.0	8.7	744.3	142.1	20180.1	2.9	11.4	99.3
Mar	30	274.2	681.7	20.6	661.1	191.5	36662.6	0.5	-0.8	69.8
Apr	30	219.9	771.9	22.7	749.3	178.1	31730.9	1.8	3.8	81.0
May	30	116.0	322.2	4.7	317.5	82.1	6738.8	0.9	0.6	70.8
Jun	30	46.3	150.3	0.6	149.6	41.5	1718.4	1.0	0.3	89.6
Jul	30	155.2	692.5	2.9	689.5	134.5	18103.2	2.3	7.9	86.7
Aug	30	115.6	320.3	1.4	318.9	78.6	6180.1	0.9	0.7	68.0
Sep	30	31.9	85.1	0.1	85.0	23.5	551.7	0.6	-0.4	73.5
Oct	30	47.9	120.4	9.1	111.3	30.5	929.8	0.8	0.2	63.6
Nov	30	62.6	170.2	9.7	160.5	41.6	1731.0	0.9	0.6	66.4
Dec	30	143.8	553.3	17.8	535.5	122.5	15000.8	1.6	3.0	85.2
Annual	30	126.6	199.7	73.1	126.6	31.2	973.9	0.3	0.1	24.7

In February, kurtosis peaks at 11.4, and skewness is lowest at 0.5 in March. Annual SD is 31.2; monthly SD ranges from 23.5 to 191.5. Summer, winter, and spring (Dec-May, Jul-Aug) have high rainfall, while autumn (Sep-Nov) is dry. Table 5 shows max 199.7mm and min 73.1mm annual rainfall in 30 years. Figure 6 depicts Midcentury's annual precipitation trends. Projections indicate 199.7mm (2042) and 73.1mm (2055), showing a notable downward trend.

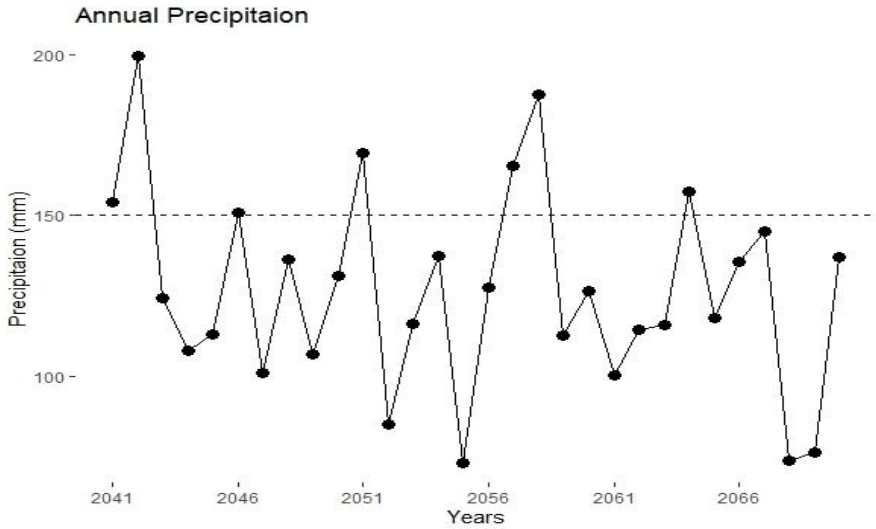

Figure 6 Annual precipitation trend for the period of midcentury (2041-2070)

Table 6 shows a significant decline in annual precipitation. Positive Kendall's tau occurred in January, March, and October, but other months had negative values. January, March, and October had a slight positive trend, while February to December exhibited a significant negative trend (95% confidence). Most months displayed a declining tendency.

Table 6 Monthly Mann-Kendall and Sen.'s slope results of precipitation in midcentury (2041-2070)

Months	Annual Precipitation			
	z-value	p-value	Kendall tau	Slope
Jan	0.93	0.35	0.12	1.76
Feb	-0.04	0.97	-0.01	-0.19

Mar	0.00	1.00	0.00	-0.04
Apr	-0.96	0.34	-0.13	-2.54
May	-0.21	0.83	-0.03	-0.48
Jun	-0.21	0.83	-0.03	-0.14
Jul	-0.25	0.80	-0.03	-0.70
Aug	-0.79	0.43	-0.10	-1.00
Sep	-0.64	0.52	-0.09	-0.30
Oct	0.61	0.54	0.08	0.34
Nov	-0.07	0.94	-0.01	-0.15
Dec	-0.61	0.54	-0.08	-1.29
Annual	-0.71	0.48	-0.09	-0.60

Temperature Trend Mid Century (2041-2070):

In Table 7, the statistically significant variables, including standard deviation, average, skewness, kurtosis, variance, range, and coefficient of variation, were calculated for the Monthly temperature data spanning from 2041 to 2070 through preliminary data analysis. During this period, the highest recorded temperature was 18.9°C in July, while the lowest recorded temperature plummeted to -4.9°C in January. Across the year, the average monthly temperature fluctuated between -1.9°C and 14.1°C. July witnessed the highest average temperature, whereas February experienced the lowest. It is worth noting that the annual standard deviation remained constant at 1.0, whereas the monthly standard deviation varied between 1.32 and 3.71.

Table 7 Monthly Temperature statistics in midcentury (2041-2070)

Months	N	Mean	Max	Min	Range	Std.D	Var	Skew	Kurt	CV%
Jan	30	-1.8	1.9	-4.9	6.8	1.7	3.0	0.3	-0.5	-93.9
Feb	30	-1.9	0.6	-4.6	5.2	1.4	2.0	0.1	-0.9	-74.7
Mar	30	0.9	3.4	-3.8	7.2	1.7	2.8	-1.0	1.0	185.2
Apr	30	4.9	7.9	0.8	7.0	1.8	3.1	-0.1	-0.6	36.1
May	30	9.6	13.2	6.4	6.9	1.8	3.4	0.1	-0.7	19.1
Jun	30	14.0	17.1	8.3	8.8	2.2	5.0	-0.4	-0.4	15.9
Jul	30	14.1	18.9	-3.8	22.6	3.7	13.6	-4.1	20.3	26.1
Aug	30	14.0	16.7	11.5	5.1	1.3	1.7	-0.1	-0.9	9.3
Sep	30	10.4	14.0	6.3	7.6	1.7	3.0	0.2	0.4	16.5
Oct	30	6.6	12.1	1.9	10.2	2.2	4.8	0.2	0.3	33.5
Nov	30	3.2	6.9	1.0	5.9	1.7	2.8	0.7	-0.5	51.6
Dec	30	-0.5	3.1	-2.9	6.0	1.5	2.2	0.5	0.0	-308.6
Annual	30	6.1	8.5	4.2	4.4	1.0	1.0	0.3	-0.3	16.6

The region's annual temperature distribution showed both positive and negative skewness, indicating unevenness. Monthly temperature CV ranged from -308.6% to 185.2%, peaking in Mar and lowest in Dec. Kurtosis values ranged from -0.9 to 20.3: Jan-Feb, Apr-Aug, and Nov had flat distributions, while other months were more peaked. Table 7 presents the statistical parameters pertaining to both monthly and annual averages.

Figure 7 illustrates the variation in average yearly temperature data across the midcentury era. The projected highest mean temperature for the year 2069 is anticipated to be 8.5°C, while the minimum is likely to be 4.8°C in 2042. The temperature in the area exhibited a notable upward trend throughout the specified time period.

Figures 8 and 9 depict the trends in mean annual maximum temperature and lowest temperature, respectively. Figure 4.7 displays a notable upward trend during the specified time period. The mean maximum temperature exhibited fluctuations, ranging from 18.9°C in 2069 to 12.8°C in 2043. Figure 9 illustrates a discernible upward trend over the specified time period.

The mean lowest temperature exhibited fluctuations, ranging from -4.9°C in 2045 to -0.2°C in 2064.

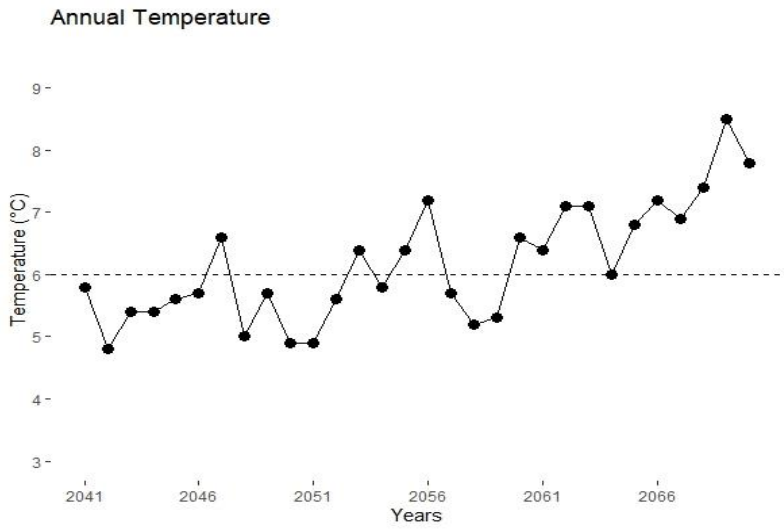

Figure 7 Annual Temperature trend for the period of midcentury (2041-2070)

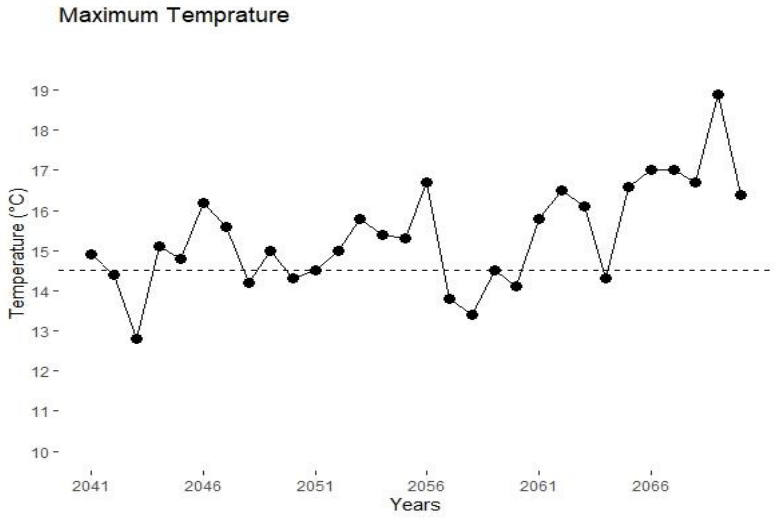

Figure 8 Annual maximum temperature trend for the period of midcentury (2041-2070)

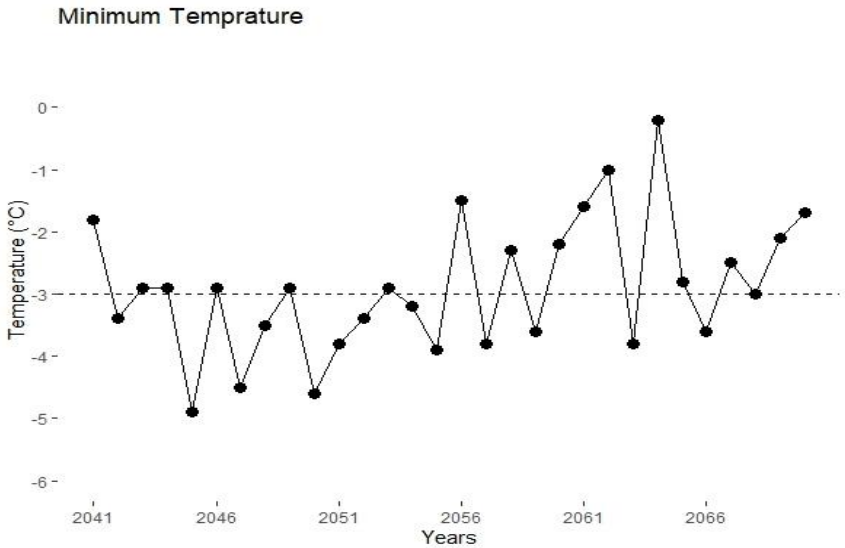

Figure 9 Annual minimum temperature trend for the period of midcentury (2041-2070)

MK and Sen's slope methods were used to analyze Jhelum Indus Basin's annual temperature data. Table 8 shows a significant upward trend in annual temperature. Positive Kendall tau values in all months indicate a 95% confidence level for the upward trend. All months display a positive slope, indicating an upward tendency.

Table 8 Monthly Mann-Kendall and Sen.'s slope results of temperature in midcentury (2041-2070)

Months	Annual Temperature			
	z-value	p-value	Kendell tau	Slope
Jan	2.43	0.02	0.31	0.09
Feb	0.43	0.67	0.06	0.02
Mar	1.11	0.27	0.14	0.04
Apr	1.86	0.06	0.24	0.07
May	1.78	0.07	0.23	0.09
Jun	3.03	0.00	0.39	0.14
Jul	1.86	0.06	0.24	0.06
Aug	1.86	0.06	0.24	0.06
Sep	2.53	2.53	0.33	0.07
Oct	3.82	0.00	0.49	0.17
Nov	3.50	0.00	0.45	0.12
Dec	2.39	0.02	0.31	0.09
Annual	4.00	0.00	0.52	0.08

Precipitation Trend End Century (2071-2099):

In the final century study, monthly rainfall data (Mean, Variance, SD, Kurtosis, Skewness, Range) was analyzed (Table 9). Rainfall varied from 51.6mm (June) to 238.1mm (March). March had the highest (840.3mm) and June the lowest (0.0mm) rainfall. CV% ranged from 55.2% (June) to 110.2% (March). Positive Skew values indicated more end-of-month rainfall.

Table 9 Monthly precipitation statistics in end century (2071-2099)

Months	N	Mean	Max	Min	Range	Std.D	Var	Skew	Kurt	CV%
Jan	29	143.5	488.6	5.3	483.3	156.5	24488.0	1.2	0.0	109.1
Feb	29	65.0	230.3	1.9	228.3	62.3	3885.0	1.3	1.1	95.9
Mar	29	238.1	840.3	7.3	833.0	205.9	42380.0	1.1	1.0	86.4
Apr	29	154.8	452.6	12.3	440.3	131.1	17178.7	1.0	-0.3	84.7
May	29	88.3	234.4	1.1	233.3	61.6	3798.3	0.6	-0.3	69.8
Jun	29	51.6	242.9	0.0	242.8	56.9	3232.6	1.7	3.5	110.2
Jul	29	158.1	465.0	13.7	451.3	103.3	10671.1	0.8	1.1	65.3
Aug	29	100.0	232.4	0.3	232.1	67.0	4494.5	0.3	-0.9	67.1
Sep	29	37.3	84.9	2.0	82.9	21.8	473.7	0.2	-0.5	58.3
Oct	29	54.8	145.4	9.9	135.5	30.2	912.6	1.2	2.1	55.2
Nov	29	69.8	204.1	5.7	198.5	46.0	2112.5	1.1	1.6	65.8
Dec	29	166.6	611.6	1.9	609.7	143.1	20487.6	1.3	2.2	85.9
Annual	29	110.7	179.3	52.1	127.2	33.1	1097.5	0.2	-0.4	29.9

In December, kurtosis peaked at 2.2, while September had the lowest skewness at 0.2. Annual SD was 33.1; monthly SD ranged from 21.8 to 205.9. Summer, winter, and spring had intense rainfall, contrasting with minimal autumn precipitation (Sep-Nov). Table 9 shows max 179.3mm and min 52.1mm annual rainfall in 29 years. Figure 10 depicts the variation in average annual precipitation. A statistically negligible declining trend in the region's precipitation data was observed.

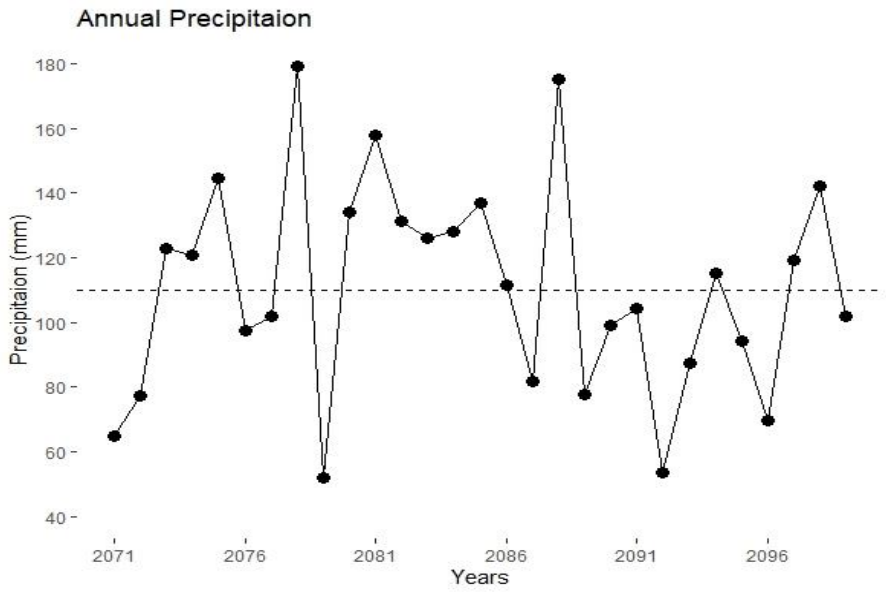

Figure 10 Annual precipitation trend for the period of end century (2071-2099)

Monthly Mann-Kendall and Sen's slope analyses were done for annual rainfall in Jhelum Indus Basin (Table 10). A statistically negligible decline in annual precipitation was observed. Positive Kendall tau values were in May, June, Sep, Nov, Dec, while negative values were in Jan, Feb, Mar, Apr, Jul, Aug, Oct. A slight positive trend was noted in May, Jun, Sep, Nov, Dec, while Jan, Feb, Mar, Apr, Jul, Aug, Oct showed a significant negative trend (95% confidence). Most months displayed a declining tendency.

Table 10 Monthly MK and Sen.'s slope results of precipitation in end century (2071-2099)

Months	Annual Precipitation			
	z-value	p-value	Kandell tau	Slope
Jan	-0.58	0.56	-0.08	-0.86
Feb	-0.51	0.61	-0.07	-0.51
Mar	-0.24	0.81	-0.03	-1.06
Apr	-0.58	0.56	-0.08	-1.22
May	0.54	0.59	0.07	0.81
Jun	1.26	0.21	0.17	1.04
Jul	-1.07	0.29	-0.14	-2.68
Aug	-0.58	0.56	-0.08	-2.68
Sep	0.00	1.00	0.00	0.01
Oct	-0.13	0.90	-0.02	-0.09
Nov	0.06	0.96	0.01	0.08
Dec	0.17	0.87	0.02	0.38
Annual	-0.51	0.61	-0.07	-0.57

Temperature Trend End Century (2071-2099):

Table 11 presents statistically significant variables like standard deviation, average, variance, skewness, range, coefficient of variation, and kurtosis for the monthly temperature series from 2071-2099. In this period, July recorded the highest temperature at 20.9°C, while January had the lowest at -6.1°C. Monthly average temperatures ranged from -0.7°C to 17.2°C, with July being the warmest and February the coldest month. The annual SD was 1.2, while monthly values varied from 1.4 to 2.9.

Table 11 Monthly temperature statistics in end century (2071-2099)

Months	N	Mean	Max	Min	Range	Std.D	Var	Skew	Kurt	CV%

Jan	29	-0.6	3.7	-3.7	7.4	1.7	2.8	0.8	0.5	-255.7
Feb	29	-0.7	4.1	-6.1	10.2	2.4	5.7	-0.4	0.3	-359.5
Mar	29	2.2	7.8	-2.3	10.1	2.0	3.9	0.2	1.8	89.6
Apr	29	7.0	11.9	2.6	9.3	2.3	5.3	0.2	-0.4	32.6
May	29	11.9	16.7	6.1	10.6	2.9	8.1	0.0	-1.0	24.0
Jun	29	16.7	20.6	11.4	9.2	1.9	3.7	-0.3	1.1	11.5
Jul	29	17.2	20.6	14.1	6.5	1.6	2.7	0.4	-0.1	9.5
Aug	29	16.2	20.9	13.0	7.9	2.0	4.1	0.3	-0.2	12.5
Sep	29	12.9	17.2	10.1	7.1	1.9	3.7	0.3	-0.7	14.8
Oct	29	8.9	13.0	4.5	8.5	1.9	3.6	-0.3	0.8	21.2
Nov	29	5.8	8.4	2.8	5.6	1.4	2.1	0.1	-0.8	24.8
Dec	29	1.3	4.2	-1.3	5.5	1.5	2.4	0.0	-1.0	116.3
Annual	29	8.2	10.2	5.8	4.4	1.2	1.4	0.0	-0.8	14.1

The annual temperature distribution exhibits both positive and negative skewness, suggesting a lack of symmetry. The CV for monthly temperatures exhibited a range of -359.5% to 116.3%, with the lowest value seen in February and the highest value observed in December. The kurtosis values spanned from -1.0 to 1.8. Specifically, the months of April-August, and Sep-Dec exhibited distributions that were relatively flat, as indicated in Table 11. Conversely, the remaining months displayed distributions that were more peaked.

Figure 11 depicts the increasing trajectory observed in the average annual temperature data throughout the last century. According to the projections, the anticipated maximum average temperature is expected to reach 10.2°C by the year 2093, while the minimum average temperature is estimated to be 5.8°C by 2076. The data presented in Figures 12 and 13 exhibit a constant upward trajectory in the average annual maximum and minimum temperatures. The observed values range from 15.1°C to 20.9°C for the mean annual maximum temperature, and from -5.6°C to 3.1°C for the mean annual minimum temperature.

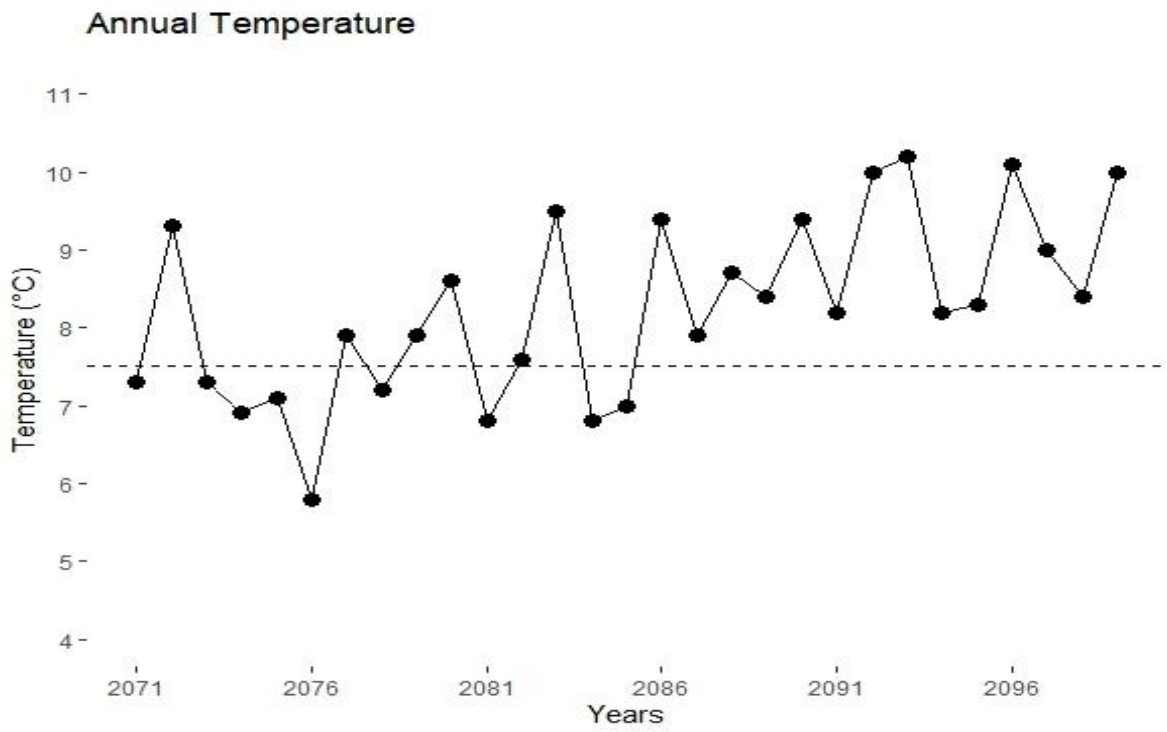

Figure 11 Annual temperature trend for the period of end century (2071-2099)

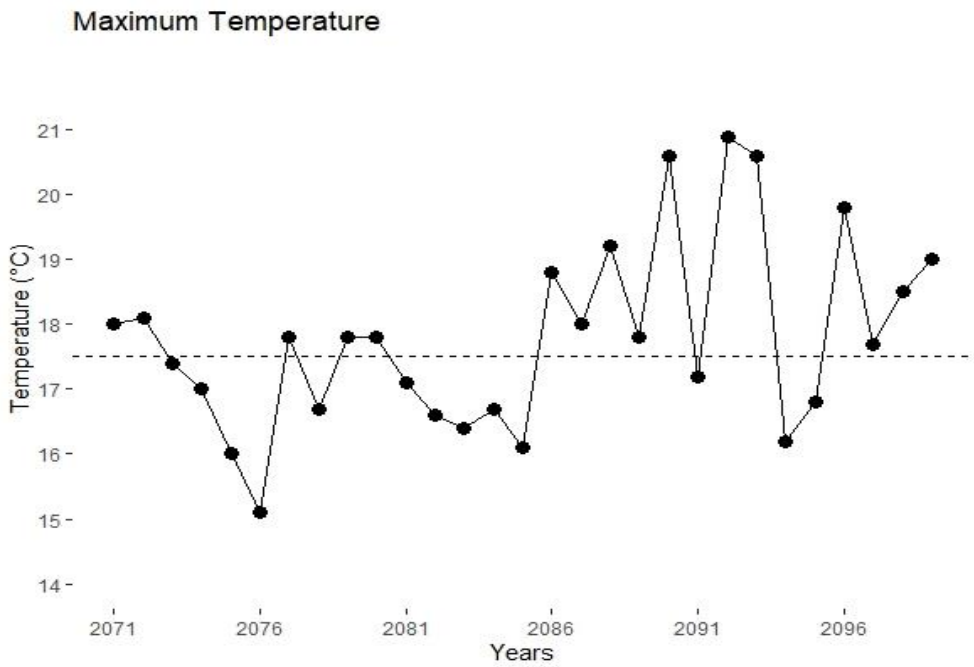

Figure 12 Annual maximum temperature trend for the period of end century (2071-2099)

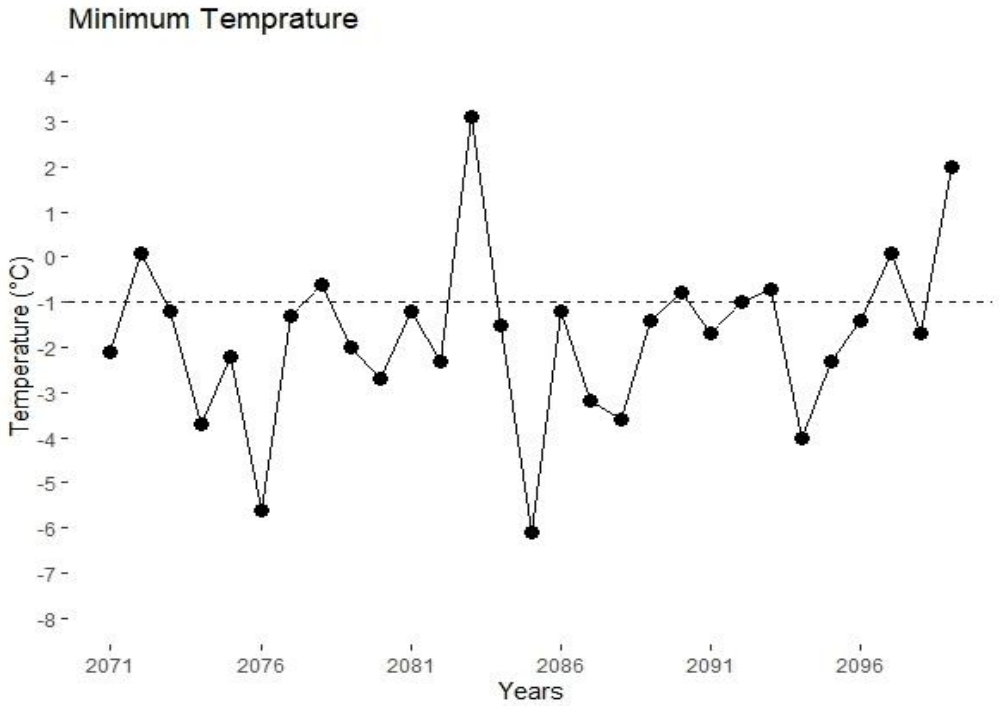

Figure 13 Annual minimum temperature trend for the period of end century (2071-2099).

The MK and Sen's slope estimate approaches were employed on a monthly basis to identify trends in the annual temperature data of the Jhelum Indus Basin. The estimation of the trend was conducted by employing the least significant level, which denotes the threshold at which the statistical significance of the trend is observed with a certain level of confidence. Table 12 exhibits a statistically significant upward trend in yearly temperature.

The p-values associated with the average months indicate the presence of a discernible trend. Positive Kendall tau values were seen in all months during the study period. During the designated period of analysis, a universally observed and statistically significant positive trend

was seen across all months, with a confidence level of 95% (α = 0.05). All months exhibit a positive slope value, indicating an upward tendency.

Table 12 Monthly MK and Sen.'s slope results of temperature in end century (2071-2099)

Months	Annual Temperature			
	z-value	p-value	Kendell tau	Slope
Jan	1.97	0.05	0.26	0.07
Feb	0.99	0.32	0.13	0.13
Mar	1.89	0.06	0.25	0.07
Apr	0.96	0.34	0.13	0.07
May	2.01	0.04	0.27	0.17
Jun	0.81	0.42	0.11	0.03
Jul	2.42	0.02	0.32	0.09
Aug	2.61	0.01	0.34	0.13
Sep	2.91	0.00	0.38	0.12
Oct	1.89	0.06	0.25	0.07
Nov	0.96	0.34	0.13	0.04
Dec	2.23	0.03	0.30	0.07
Annual	3.32	0.00	0.44	0.08

Seasonal Variation of Precipitation and Temperature for Future Period (2020-2099):

Table 13 displays the average values of precipitation and temperature for several seasonal periods during future time intervals (2020-2040, 2041-2070, 2071-2099). Over the course of the previous century, it was observed that spring had the most substantial amount of precipitation, with a recorded average rainfall of 178.6mm. Conversely, autumn exhibited the lowest levels of rainfall, with an average of 42.7mm. During the aforementioned period, the maximum precipitation recorded during spring was 203.4mm, while the minimum precipitation observed during autumn was 84.8mm. At the conclusion of the century, the spring season exhibited a precipitation measurement of 160.4mm, while the autumn season observed a precipitation measurement of 54.0mm. During the course of the investigation, it was observed that spring had the greatest amount of precipitation, while autumn demonstrated the lowest levels. The data indicates that there was a rise in precipitation towards the middle of the century, followed by a subsequent fall towards the end of the century, so implying the occurrence of a peak in precipitation during the mid-20th century.

In terms of temperature, it can be observed that the highest recorded average temperature of 12.9°C was experienced during the summer season, while the lowest recorded average temperature of -2.6°C occurred during the winter season throughout the course of the past century. During the midcentury period, the average temperature during July was recorded to be 14.0°C, while winter temperatures dropped to -1.4°C. By the conclusion of the century, the average temperature of the summer season was recorded at 16.7°C, while the winter season experienced temperatures as low as 0.0°C. Throughout all seasons, there was a noticeable increase in temperatures throughout the midcentury in comparison to the preceding century, with further escalation observed towards the conclusion of the century. In general, the data indicates a consistent increase in temperatures over the duration of the research.

Table 13 Seasonal variation of precipitation and temperature for future period (2020-2099)

Variables	Time Period	Winter	Spring	Summer	Autumn
Precipitation	2020-2040	119.9	178.6	114.5	42.7
	2041-2070	149.8	203.4	105.7	84.8
	2071-2099	125.0	160.4	103.2	54.0
Temperature	2020-2040	-2.6	4.9	12.9	5.4
	2041-2070	-1.4	5.1	14.0	6.7

2071-2099	0.0	7.1	16.7	9.2

Conclusion:

This study analyzes temperature and precipitation data from 2020 to 2099. From 2020 to 2040, monthly precipitation varied (30.4mm in September to 253.1mm in March) and temperatures fluctuated (-3.1°C in January to 13.4°C in July). There's a minimal upward trend but not statistically significant. In the midcentury (2041-2070), March had the highest rainfall (274.2mm), and September the lowest (31.9mm). There was a notable decrease in precipitation and a corresponding temperature increase during this period. From 2071 to 2099, March had the highest average rainfall, and June had the lowest. The basin exhibited a statistically significant temperature increase over the final century. Precipitation patterns showed an upward tendency in midcentury followed by a decline toward the end. Spring had the most rainfall, and autumn had the least throughout the study periods. The examination of temporal fluctuations in rainfall and temperature throughout prospective timeframes spanning from 2020 to 2099 unveils intriguing patterns. The observed patterns indicate that there is an upward tendency in precipitation levels throughout the midcentury era in comparison to the preceding near century, followed by a subsequent decline in precipitation levels towards the conclusion of the century. The data indicates a constant upward trend in temperature values from the early part of the century to the middle, followed by a subsequent increase from the middle to the end of the century. Furthermore, the data revealed that the highest amount of precipitation is experienced during the spring season, whereas the lowest amount of rainfall is recorded during autumn throughout all temporal intervals.

References:

[1] M. DEMİRCAN, H. GÜRKAN, O. ESKİOĞLU, H. ARABACI, and M. COŞKUN, "Climate Change Projections for Turkey: Three Models and Two Scenarios," Turkish J. Water Sci. Manag., vol. 1, no. 1, pp. 22–43, Jan. 2017, doi: 10.31807/TJWSM.297183.

[2] Z. P. Xu, Y. P. Li, G. H. Huang, S. G. Wang, and Y. R. Liu, "A multi-scenario ensemble streamflow forecast method for Amu Darya River Basin under considering climate and land-use changes," J. Hydrol., vol. 598, p. 126276, Jul. 2021, doi: 10.1016/J.JHYDROL.2021.126276.

[3] H. Deng, Y. Chen, H. Wang, and S. Zhang, "Climate change with elevation and its potential impact on water resources in the Tianshan Mountains, Central Asia," Glob. Planet. Change, vol. 135, pp. 28–37, Dec. 2015, doi: 10.1016/J.GLOPLACHA.2015.09.015.

[4] F. Giorgi and P. Lionello, "Climate change projections for the Mediterranean region," Glob. Planet. Change, vol. 63, no. 2–3, pp. 90–104, Sep. 2008, doi: 10.1016/J.GLOPLACHA.2007.09.005.

[5] H. Rodhe, "A comparison of the contribution of various gases to the greenhouse effect," Science, vol. 248, no. 4960, pp. 1217–1219, 1990, doi: 10.1126/SCIENCE.248.4960.1217.

[6] J. Stephenson, K. Newman, and S. Mayhew, "Population dynamics and climate change: what are the links?," J. Public Health (Bangkok)., vol. 32, no. 2, pp. 150–156, Jun. 2010, doi: 10.1093/PUBMED/FDQ038.

[7] E. J. Kweka, E. E. Kimaro, and S. Munga, "Effect of deforestation and land use changes on mosquito productivity and development in western kenya highlands: Implication for malaria risk," Front. Public Heal., vol. 4, no. OCT, p. 208939, Oct. 2016, doi: 10.3389/FPUBH.2016.00238/BIBTEX.

[8] S. Ali et al., "Corrigendum to 'Assessment of climate extremes in future projections downscaled by multiple statistical downscaling methods over Pakistan' [Atmospheric Research 222 (2019) 114–133]," Atmos. Res., vol. 224, p. 196, Aug. 2019, doi:

10.1016/J.ATMOSRES.2019.03.030.

[9] T. Andrews et al., "Accounting for Changing Temperature Patterns Increases Historical Estimates of Climate Sensitivity," Geophys. Res. Lett., vol. 45, no. 16, pp. 8490–8499, Aug. 2018, doi: 10.1029/2018GL078887.

[10] F. Nordio, A. Zanobetti, E. Colicino, I. Kloog, and J. Schwartz, "Changing patterns of the temperature-mortality association by time and location in the US, and implications for climate change," Environ. Int., vol. 81, pp. 80–86, Aug. 2015, doi: 10.1016/J.ENVINT.2015.04.009.

[11] T. Ben-Gai, A. Bitan, A. Manes, P. Alpert, and S. Rubin, "Temporal and spatial trends of temperature patterns in Israel," Theor. Appl. Climatol., vol. 64, no. 3–4, pp. 163–177, 1999, doi: 10.1007/S007040050120/METRICS.

[12] C. Huntingford, P. D. Jones, V. N. Livina, T. M. Lenton, and P. M. Cox, "No increase in global temperature variability despite changing regional patterns," Nat. 2013 5007462, vol. 500, no. 7462, pp. 327–330, Jul. 2013, doi: 10.1038/nature12310.

[13] J. M. Gregory and J. Oerlemans, "Simulated future sea-level rise due to glacier melt based on regionally and seasonally resolved temperature changes," Nat. 1998 3916666, vol. 391, no. 6666, pp. 474–476, Jan. 1998, doi: 10.1038/35119.

[14] A. A. Tahir, P. Chevallier, Y. Arnaud, L. Neppel, and B. Ahmad, "Modeling snowmelt-runoff under climate scenarios in the Hunza River basin, Karakoram Range, Northern Pakistan," J. Hydrol., vol. 409, no. 1–2, pp. 104–117, Oct. 2011, doi: 10.1016/J.JHYDROL.2011.08.035.

[15] M. Hassan, P. Du, R. Mahmood, S. Jia, and W. Iqbal, "Streamflow response to projected climate changes in the Northwestern Upper Indus Basin based on regional climate model (RegCM4.3) simulation," J. Hydro-environment Res., vol. 27, pp. 32–49, Dec. 2019, doi: 10.1016/J.JHER.2019.08.002.

[16] A. F. Lutz, W. W. Immerzeel, P. D. A. Kraaijenbrink, A. B. Shrestha, and M. F. P. Bierkens, "Climate Change Impacts on the Upper Indus Hydrology: Sources, Shifts and Extremes," PLoS One, vol. 11, no. 11, p. e0165630, Nov. 2016, doi: 10.1371/JOURNAL.PONE.0165630.

[17] A. J. Khan, M. Koch, and A. A. Tahir, "Impacts of Climate Change on the Water Availability, Seasonality and Extremes in the Upper Indus Basin (UIB)," Sustain. 2020, Vol. 12, Page 1283, vol. 12, no. 4, p. 1283, Feb. 2020, doi: 10.3390/SU12041283.

[18] A. A. Tahir, J. F. Adamowski, P. Chevallier, A. U. Haq, and S. Terzago, "Comparative assessment of spatiotemporal snow cover changes and hydrological behavior of the Gilgit, Astore and Hunza River basins (Hindukush–Karakoram–Himalaya region, Pakistan)," Meteorol. Atmos. Phys., vol. 128, no. 6, pp. 793–811, Dec. 2016, doi: 10.1007/S00703-016-0440-6.

[19] A. F. Lutz, W. W. Immerzeel, A. B. Shrestha, and M. F. P. Bierkens, "Consistent increase in High Asia's runoff due to increasing glacier melt and precipitation," Nat. Clim. Chang. 2014 47, vol. 4, no. 7, pp. 587–592, Jun. 2014, doi: 10.1038/nclimate2237.

[20] T. G. Andualem, D. A. Malede, and M. T. Ejigu, "Performance evaluation of integrated multi-satellite retrieval for global precipitation measurement products over Gilgel Abay watershed, Upper Blue Nile Basin, Ethiopia," Model. Earth Syst. Environ., vol. 6, no. 3, pp. 1853–1861, Sep. 2020, doi: 10.1007/S40808-020-00795-W/METRICS.

[21] S. A. Diress and T. B. Bedada, "PRECIPITATION AND TEMPERATURE TREND ANALYSIS BY MANN KENDALL TEST: THE CASE OF ADDIS ABABA METHODOLOGICAL STATION, ADDIS ABABA, ETHIOPIA," African J. L. Policy Geospatial Sci., vol. 4, no. 4, pp. 517–526, Sep. 2021, doi: 10.22004/AG.ECON.334454.

[22] M. Rizwan et al., "Simulating future flood risks under climate change in the source region of the Indus River," J. Flood Risk Manag., vol. 16, no. 1, p. e12857, Mar. 2023, doi: 10.1111/JFR3.12857.

[23] D. R. Archer, N. Forsythe, H. J. Fowler, and S. M. Shah, "Indus basin water resources sustainability Sustainability of water resources management in the Indus Basin under changing climatic and socio economic conditions Indus basin water resources sustainability," Hydrol. Earth Syst. Sci. Discuss, vol. 7, pp. 1883–1912, 2010, Accessed: Sep. 28, 2023. [Online]. Available: www.hydrol-earth-syst-sci-discuss.net/7/1883/2010/